MATERIALS CHARACTERIZATION 62 (2011) 367–372

available at www.sciencedirect.com

ScienceDirect

www.elsevier.com/locate/matchar

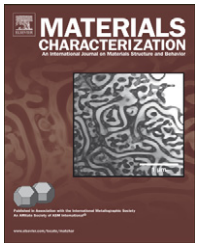

Microstructures and properties of low cycle fatigue of electrolytic A356 alloys

*Song Mousheng**, *Ran Maowu*

Department of Physics and Electronics Science, Tongren University, Tongren 554300, China

ARTICLE DATA

Article history:
Received 4 July 2010
Received in revised form
23 January 2011
Accepted 26 January 2011

Keywords:
A356 alloys
Cyclic hardening
Fatigue life
Microstructure

ABSTRACT

Microstructures and properties of low cycle fatigue of electrolytic A356 cast alloys with different Ti contents were investigated, and corresponding properties of melting A356 alloys were also investigated as a comparison. All tested alloys exhibited the evident cyclic hardening behavior, and the alloys with 0.14% Ti had the higher cyclic hardening rate than the alloys with 0.10% Ti. When tested at higher strain amplitudes, the cyclic stress amplitudes of electrolytic alloys remained basically in the quasi-stable state, while the cyclic stress amplitudes of melting alloys continuously proceeded. The fatigue life of the A356 alloy was controlled by Ti content instead of the Ti-addition method. In comparison to the alloys with 0.14% Ti, the alloy with 0.10% Ti exhibited the longer fatigue life due to its lower yield stress. The fatigue flats, coupled with some fatigue striations and fatigue slipbands, were observed to occur in the fracture surfaces of the electrolytic A356 alloy at lower strain amplitudes.

1. Introduction

A356 alloys have been paid increasing attention in the automobile and aerospace industries as the potential advanced engineering structural materials by virtue of the excellent casting and heat treatment properties, high machinability and fatigue performance, as well as the good strength and plasticity [1]. Numerous papers about A356 alloys have focused on the grain refinement, melt processing and microstructure fading, and also the hardness and strength, wear resistance, static or quasi-static etc normal mechanical properties. However, very limited data on fatigue resistance have been reported on these alloys especially under T6 condition with different Ti-addition methods and Ti content. The microstructure plays an important role in determining the fatigue properties of materials. It has been reported [2,3] that refining the microstructure and modifying the eutectic silicon particles are favorable to prolong the fatigue life of the alloys. In light of the practical service status of the materials, most materials suffer the cyclic loading and the fatigue damage is still the primary failure modes of mechanical parts and engineering components. Therefore, in many cases, the fatigue fracture is a crucial factor to influence the service life of the materials. Under alternating loading, the fatigue service properties of the materials are usually controlled by the cyclic plastic deformation at the stress concentration position [4]. So, it is of considerable interests to investigate the fatigue properties, especially the low cycle fatigue (LCF) properties of the A356 cast alloys.

Ti-addition by electrolysis is a novel and promising method of Ti-alloying developed in the recent years, which directly produces the low-titanium aluminum alloys by adding some TiO_2 into an electrolyzer. In comparison to the traditional Ti-addition method, namely the melting master alloys, the method of electrolysis exhibits many advantages [5,6], such as the lower costs of Ti-alloying, the refiner grains, the higher fading resistance and the easier composition-controlling. In this study, the LCF experiments of the electrolytic A356 cast alloys with different Ti content (*mass.*%) were carried out and their fracture features were analyzed. As a comparison, the

* *Corresponding author*. Tel./fax: +86 856 5213605.
E-mail address: sms071201@163.com (S. Mousheng).

1044-5803/$ – see front matter © 2011 Elsevier Inc. All rights reserved.
doi:10.1016/j.matchar.2011.01.015

LCF properties of the melting A356 cast alloys were investigated too.

2. Experimental Procedures

The A356 alloys with 0.1 and 0.14% Ti content were produced by different Ti-addition method, namely the electrolysis and melting method. The electrolytic A356 alloys (E10, E14) were directly fabricated by in-situ titanium alloying Al-0.18% Ti alloys that were produced by electrolysis. The melting A356 alloys (M10, M14) were casted by melting Al-5% Ti master alloys and pure Al. The chemical compositions of all tested A356 alloys are listed in Table 1.

The casted samples were heat treated by T6 technology (Solution for 6 h × 535 °C and aging for 8 h × 165 °C), and then were machined into the tensile specimen ($\Phi 8 \times 80$) and the standard fatigue specimen ($\Phi 8 \times 16$). Afterwards, the tensile and LCF tests were conducted at room temperature using the hydraulic servo material tester (Model MTS-810, MTS, USA). The tensile test was performed with a rate of 2 mm/min, and its corresponding mechanical properties are listed in Table 2. The LCF experiment was carried out with a reversed triangular wave (strain ratio $R=-1$ and frequency $f=1.0$ Hz). The half strain amplitudes are $\Delta\varepsilon_t/2 = 0.9\%, 0.7\%, 0.5\%, 0.3\%, 0.25\%$, respectively.

The metallographic microstructures were determined by Nikon MBA21000 (Olympus, Japan) and were quantitatively analyzed by WD-5 system (Wuhan University, China). The microtructure parameters such as primary dendrite length (PDL), second dendrite arm spacing (SDAS), as well as Si particle sizes are also listed in Table 2. The observation of fracture surface of tested alloys was conducted by a scanning electron microscopy (SEM) (Model JSM-5610LV, Jeol, Japan). A transmission electron microscopy (Model H-800, Hitachi, Japan) was employed to observe the dislocation cell of fatigue specimen.

3. Results and Discussion

Under cyclic loading, the stress–strain ($\sigma-\varepsilon$) plot is out of the elastic range and enters into the plastic region, so the total half strain amplitude ($\Delta\varepsilon_t/2$) consists of the elastic half strain amplitude ($\Delta\varepsilon_e/2$) and the plastic half strain amplitude ($\Delta\varepsilon_p/2$). Fig. 1 shows the cyclic $\sigma-\varepsilon$ plots of the tested A356 alloys, viz. E10, E14, M10 and M14. Their corresponding $\sigma-\varepsilon$ plots obtained by monotonic tensile tests are also shown as a comparison. As indicated, all tested alloys exhibited the evident cyclic hardening phenomenon. No matter the Ti-addition method, raising Ti content can greatly increase the cyclic hardening capacity. The alloys with higher Ti content appear to have the stronger cyclic hardening capacity in virtue of the better grain refinement, the higher yield strength and tensile strength (as listed in Table 2). At higher $\Delta\varepsilon_t/2$, the cyclic hardening trend of the electrolytic A356 alloy exhibits a quasi-stable deformation state, while the cyclic hardening trend of the melting A356 alloy continuously proceed and has no appearance of a quasi-stable state.

Table 1 – Chemical compositions of A356 alloys (*mass.%*).

Sample	Ti-addition method	Ti	Si	Fe	Mg	Sr	Al
E10	By electrolysis	0.105	6.57	0.100	0.380	0.027	Bal.
E14	By electrolysis	0.139	6.87	0.099	0.405	0.025	Bal.
M10	By melting	0.098	6.63	0.102	0.385	0.026	Bal.
M14	By melting	0.137	6.89	0.103	0.406	0.025	Bal.

It has been reported that the solidification microstructure and aging condition played an important role in determining the cyclic hardening behavior of the materials. The interaction among dislocations, eutectic particles, and also dendrite cell/grain boundaries all has a strong influence on the cyclic hardening behavior [7]. As seen in Table 2, the tested A356 alloys with different Ti-addition methods have the similar SDAS, but the refinement effect of grain and morphologies of silicon particles among the tested alloys are rather distinguishing. The cyclic hardening behavior of alloys with finer microstructure is mainly controlled by the dendrite cell size or grain size. Because the dislocation slip distance is closely related to the dendrite cell size or grain size, refining the grain can enhance the resistance of dislocation crossing the grain boundaries, which leads to the increase of the cyclic hardening capacity of the A356 alloys. Han [7] had ever confirmed that refining the microstructure could facilitate the cyclic hardening trend of alloys under low cycle loading when SDAS was less than 60 μm.

The morphologies of dislocation cell of the electrolytic A356 alloy at different $\Delta\varepsilon_t/2$ is displayed in Fig. 2. As shown, with the number of cycles increasing, the density of dislocation gradually increases and the entanglement of dislocation becomes stronger, which enhances the resistance of subsequent dislocation movement and gives rise to the intense cyclic hardening capacity. Under alternating loading, alloys will occur to cyclic deformation, leading the ability of dislocation cross-slip to be unceasingly strengthened. Because the resistance of dislocation cross-slip comes from the boundary between Si particles and grains, the refiner grains will shorten the mean free path of dislocation slipping and thus result in the higher cyclic hardening capacity. In Table 2, the electrolytic A356 alloys have the refiner grains, the better grain distributions and the morphologies of Si particles than the melting A356 alloys, so the dislocations easily pile-up, entangle and reach to a quasi-stable state at lower strain amplitude.

The cyclic $\sigma-\varepsilon$ correlation can be quantitatively expressed by Hollomon equation:

$$\frac{\Delta\varepsilon_t}{2} = \frac{\Delta\sigma_t}{2E} + \left(\frac{\Delta\sigma_t}{2K}\right)^{\frac{1}{n}} \left(\text{where}\ \frac{\Delta\sigma_t}{2} = K\left(\frac{\Delta\varepsilon_p}{2}\right)^n\right) \quad (1)$$

where $\Delta\sigma_t/2$ denotes the total half stress amplitude at stable loading, E is the elasticity modulus, K is the coefficient of cyclic strength and n is the hardening exponent of cyclic strain. Generally, high K value means the higher strength of materials, and high n value denotes the faster cyclic hardening rate, the higher plastic deformation resistance and the lower ductility. The LCF cyclic hardening (or softening) behavior of metallic materials is linked to its corresponding tensile testing. By fitting

Table 2 – Mechanical properties and microstructure parameters of A356 alloys.

Sample	σ_s/MPa	σ_b/MPa	δ/%	K/MPa	n	PDL/μm	SDAS/μm	Average diameter of Si particles/μm	Roundness of Si particles
E10	248.1	319.3	8.6	335	0.115	197.8	24.2	2.592	0.877
E14	261.0	327.8	7.1	378	0.154	190.1	23.7	2.539	0.911
M10	254.4	319.6	6.7	345	0.141	204.2	24.8	2.699	0.858
M14	267.0	327.6	6.3	380	0.144	197.3	24.1	2.651	0.891

Eq. (1), it can obtain the values of K and n of the tested A356 alloys as listed in Table 2 too. Except for E10 alloy, the range of n values is 0.14–0.15 for M10, E14 and M14 alloys, which is in accordance with those of most metals (n=0.1–0.2)[?]. Landgraf [8] considered that the cyclic softening at $n<0.1$, the cyclic stability at $n=0.1$ and the cyclic hardening at $n>0.1$ appeared respectively. In Table 2, the K values of tested alloys with same Ti content (E10 and M10, E14 and M14) are equivalent, meaning the similar strength, while the n value of E10 alloy is far less than those of the others due to its higher plasticity. Low n value indicates the slower cyclic hardening rate and better ductility. Under invariable strain loading, if the material exhibits cyclic hardening, the stress will become more and more strong, which leads the loading components to early fracture.

The cyclic strain–life ($\Delta\varepsilon-N_f$) correlation is an important aspect to characterize the fatigue behavior of materials, and also is a key factor to improve the fatigue service properties. The LCF $\Delta\varepsilon-N_f$ curve is usually figured by the total half strain amplitude and the number of reversals to failure in log–log coordinates, namely $\Delta\varepsilon_t/2-2N_f$. Accordingly, both $\Delta\varepsilon_e/2-2N_f$ and $\Delta\varepsilon_p/2-2N_f$ can be figured in log–log coordinates too. Fig. 3 reveals the cyclic $\Delta\varepsilon_t/2-2N_f$, $\Delta\varepsilon_e/2-2N_f$ and $\Delta\varepsilon_p/2-2N_f$ curves of four A356 alloys. Whether Ti-addition by electrolysis or by melting, alloys with 0.10% Ti have the longer LCF life than alloys with 0.14% Ti, suggesting the less effect of Ti-addition method on LCF life of alloys. Additionally, alloys with the same Ti-addition method exhibit the similar elastic fatigue life and the distinct plastic fatigue life, which indicates that LCF life is mainly controlled by the plastic strain rather than the elastic strain.

In Fig. 3, N_t, is the transition fatigue life, namely the fatigue life at the intersection between $\Delta\varepsilon_e/2-2N_f$ and $\Delta\varepsilon_p/2-2N_f$ curves, where the damage brought by the elastic strain is equal to that by the plastic strain at $\Delta\varepsilon_e=\Delta\varepsilon_p$. When $N_f<N_t$ and $\Delta\varepsilon_p>\Delta\varepsilon_e$, the plastic strain dominantly operates under cyclic loading and the fatigue resistance is mainly controlled by the materials plasticity. While $N_f>N_t$ and $\Delta\varepsilon_p<\Delta\varepsilon_e$, LCF is dominated by the elastic strain and the fatigue resistance is determined by the strength. In Fig. 3, A356 alloys with 0.10% Ti and 0.14% Ti have similar elastic fatigue life, meaning the equivalent strength. However, alloys with 0.10% Ti exhibit the better ductility, giving rise to the longer transition fatigue life N_t.

It was not the prime dendrite length (PDL) but the second dendrite arm spacing (SDAS) had a great effect on determining the fatigue life of materials [9]. In Table 2, both the Ti-addition method and Ti content have less influence on the SDAS, and SDAS of all tested alloys are 24 μm or so, which is in good accordance with Zhang's work [10]. Zhang performed the LCF testing of A356 alloys and demonstrated that LCF life was insensitive to the solidification microstructures of alloys when SDAS is less than 30 μm.

The yield strength of materials has a great influence on its fatigue life. If the yield strength is low, the stress concentration generating from the non-uniform region easily relaxes through the local plastic deformation, and thus delays the nucleation of fatigue micro-crack [11]. Han proved that the

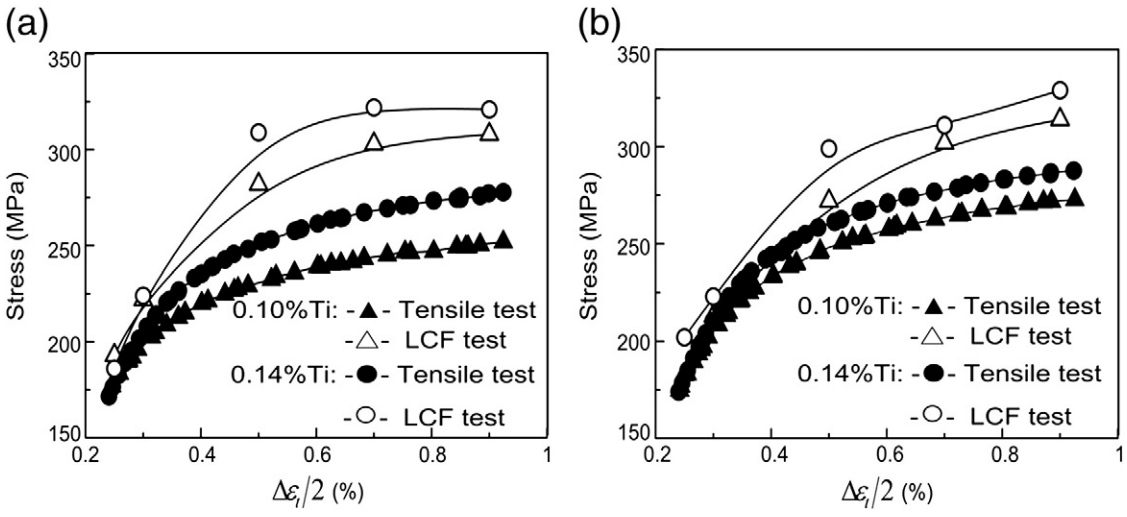

Fig. 1 – Cyclic $\sigma-\varepsilon$ plots of A356 alloys with different Ti-addition method: (a) by electrolysis and (b) by melting Al-5% Ti master alloys.

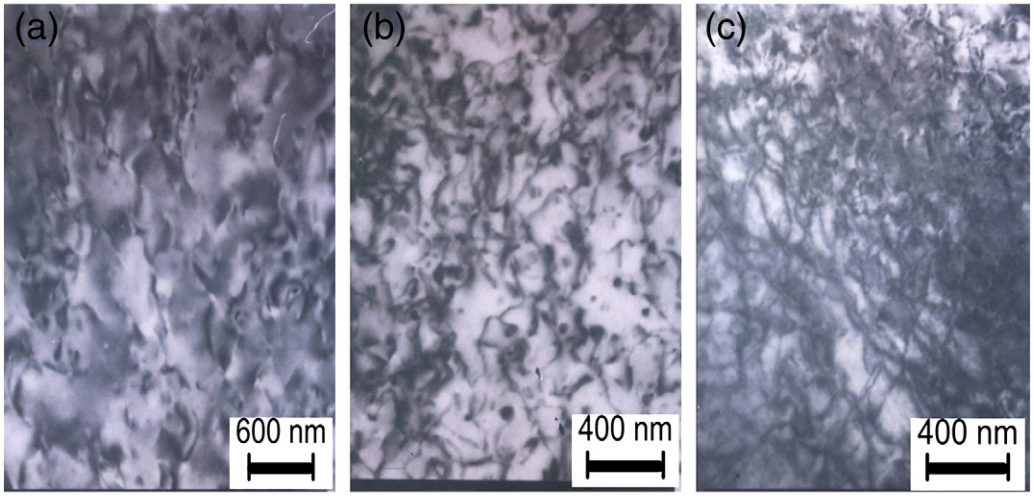

Fig. 2 – TEM morphologies of the dislocation of electrolytic A356 alloy at different $\Delta\varepsilon_t/2$: (a) $\Delta\varepsilon_t/2=0.7\%$, (b) $\Delta\varepsilon_t/2=0.5\%$ and (c) $\Delta\varepsilon_t/2=0.3\%$.

size of the cyclic plastic region near the crack-tips was inversely proportional to the square of the yield strength [7]. Additionally, according to the research on the cyclic strain fatigue behavior of A356 alloy [12], the relationship between the size of the cyclic plastic region at the crack-tips and the yield strength meets the equation:

$$r_c = 0.11\left(\frac{K^{tr}_{max}}{\sigma_s}\right) \quad (2)$$

where r_c denotes the size of the cyclic plastic region, $K^{tr}_{max}$is the maximum stress strength factor and σ_s is the yield stress, respectively. Clearly, the lower yield stress, the higher size of local plastic deformation, it will lead to the higher plasticity-induced closure-crack and increase the crack-propagating resistance. At the same time, the higher plastic deformation region at the crack-tips can also enhance the resistance of dislocation movement forced by the matrix. Accordingly, it will prevent the dislocation from moving to crystal cell or grain boundary and interacting with eutectic particles, which results in the decrease of crack-propagating velocity and the improvement of the fatigue life of alloys. As listed in Table 2, the alloys with same Ti have the similar yield stress σ_s, but the σ_s of alloys with low Ti (E10, M10) are lower than those of alloys with high Ti (E14, M14). So, according to Eq. (2), the size of the cyclic plastic region at the crack-tips of E10 and M10 alloys is larger than those of E14 and M14 alloys, and hence its plasticity-induced closure-crack ability is greatly higher than that of the latter. As a result, the former exhibits a higher resistance of fatigue crack propagation and a lower propagation velocity, giving rise to the longer LCF life.

Fig. 4 shows the microstructures of the fracture surfaces of E10 alloy at various $\Delta\varepsilon_t/2$. At high $\Delta\varepsilon_t/2$, the surface exhibits dimples-like and tearing-edges fracture feature, suggesting its similarity to the tensile fracture. At high strain amplitude, the micro-crack primarily initiates from the grain boundary and propagates along the grain boundary and the eutectic phase

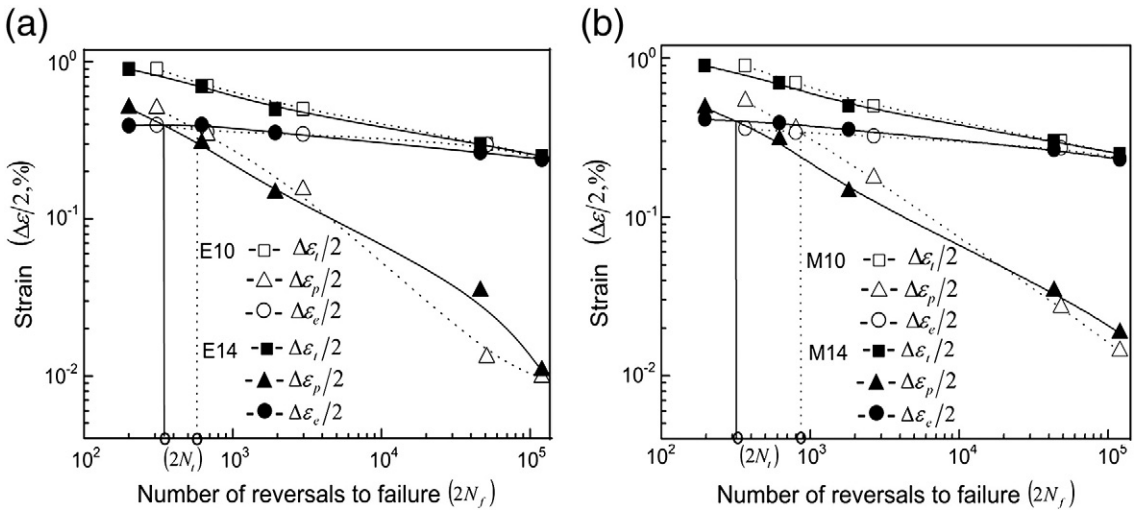

Fig. 3 – Cyclic $\Delta\varepsilon/2-2N_f$ curves of A356 alloys with different Ti-addition method: (a) by electrolysis and (b) by melting Al-5% Ti master alloys.

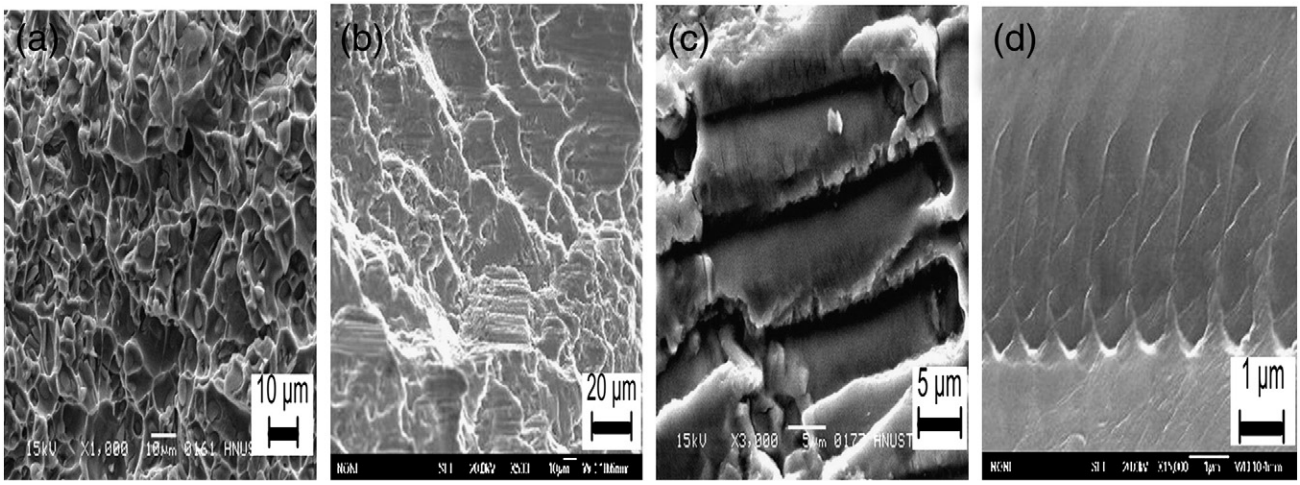

Fig. 4 – Microstructures of the fracture surfaces of E10 alloy at different $\Delta\varepsilon_t/2$: (a) dimples ($\Delta\varepsilon_t/2=0.7\%$), (b) flats ($\Delta\varepsilon_t/2=0.5\%$), (c) striations ($\Delta\varepsilon_t/2=0.3\%$) and (d) slipbands ($\Delta\varepsilon_t/2=0.3\%$).

boundary, where the incompatibility of local deformation is rather evident and the resistance of crack propagation is lower. Once the micro-crack initiates, it would rapidly propagate, which displays the mono-crack initiator characters and leads to the lower LCF life.

At low strain amplitude, however, there appear some flats (Fig. 4b) on the fracture surface. The tyre-like striations are obviously observed (Fig. 4c) on the flats, and each striations exhibits a propagation period of fatigue crack under cyclic loading. The tyre-like striation corresponds to the blunting–sharpening (B–S) trace of fatigue micro-crack tips in microstructure, and its appearance means the increase of resistance of fatigue cracks propagation due to the higher ductility of alloy, resulting in a longer fatigue life. Moreover, there exists a vast of fatigue slipbands with the regular array (Fig. 4d). Obviously, at low $\Delta\varepsilon_t/2$, Al(α) matrix at the crack-tips undergoes a severe plastic deformation during the fatigue micro-cracks initiating and then propagating. Because Al(α) matrix belongs to the faced-centered cubic (*fcc*) lattice and has a higher stacking fault energy, it has a number of propagated slipping systems $\{111\}\langle 110\rangle$ and the critical resolved shear stress is rather low. Under cyclic loading, even if bearing the lower plastic deformation, the dislocation could initiate easily and occur to cross-slip, resulting in the non-uniform deformation of parts and a large number of fatigue flats and striations.

Additionally at low $\Delta\varepsilon_t/2$, the micro-crack initiators usually nucleate from the defects such as the inclusions, pores, notches and irregular Si particles [13], as well as the non-uniform deformation of grains, and the failure exhibits a typical multistage fatigue crack growth feature [14]. Under alternating loading of high cycles, once the crack initiates, the multistage fatigue crack will propagate and grow through the Al(α) matrix by B–S manner. For each B–S process, the dislocation will occur to cross-slip, pile-up and entangle inside the crack-tips plastic region. As a consequence, once the alloys fracture, the evident fatigue flats and striations, even the fatigue slipbands, are clearly observed on the fracture surfaces.

4. Conclusions

Both the electrolytic and melting A356 alloys exhibited the evident cyclic hardening behavior. The LCF life of alloys were only sensitive to Ti content and the A356 alloys with 0.10% Ti had the longer LCF life in comparison to alloys with 0.14% Ti. The fatigue flats, striations and slipbands were observed on the fracture surfaces at lower strain amplitudes.

Acknowledgements

This work was financially supported by the Science and Technology Foundation of Guizhou Province of China under grant no.J20102016. And also the authors would like to acknowledge the Research Fund of Tongren University under grant no. TR084 for the financial support.

REFERENCES

[1] Emami AR, Begum S, Chen DL. Cyclic deformation behavior of a cast aluminum alloy. Mater Sci Eng 2009;A516:31–41.
[2] Wang QG, Apelian D. Fatigue behavior of A356/357 aluminum cast alloys. Part II—Effect of microstructural constituents. J Light Met 2001;1:85–97.
[3] De PS, Mishra RS, Smith CB. Effect of microstructure on fatigue life and fracture morphology in an aluminum alloy. Scr Mater 2009;60:500–3.
[4] Ganesh S, Raman S. On cyclic stress–strain behaviour and low cycle fatigue life. Mater Design 2002;23:249–54.
[5] Wang RY, Lu WH, Hogan LM. Self-modification in direct electrolytic Al–Si alloys (DEASA) and its structural inheritance. Mater Sci Eng 2003;A348:289–98.
[6] Liu ZX, Wang MX, Song TF. The production and the mechanical properties of in-situ Titanium alloying A356 alloys. Mater Sci Forum 2005;475–479:321–4.

[7] Han SW, Katsumata K. Effects of solidification structure and aging condition on cyclic stress–strain response in Al-7%Si-0.4%Mg cast alloys. Mater Sci Eng 2002;A337:170–8.
[8] Landgraf RW. Achievement of high fatigue resistance in metals and alloys. ASTM STP 1970;3:467–70.
[9] Han SW, Shinji KS. Fatigue crack growth behavior in semi-liquid die-cast Al-7%Si-0.4%Mg alloys with fine effective grain structure. Mater Sci Eng 2001;A308:225–32.
[10] Zhang B, Chen W, Poirier DR. Effect of solidification cooling rate on the fatigue life of A356.2-T6 cast aluminium alloy. Fatigue Fract Eng Mater Struct 2000;23:417–23.
[11] Zhang XP, Li JC, Wang CH. Prediction of short fatigue crack propagation behaviour by characterization of both plasticity and roughness induced crack closures. Int J Fatigue 2002;24:529–36.
[12] Gall K, Yang N. The influence of modified intermetallics and Si particles on fatigue crack paths in a cast A356 Al alloy. Fatigue Fract Eng Mater Struct 2000;23:159–72.
[13] Fan JH, Mcdowell DL, Horstemeyer MF. Cyclic plasticity at pores and inclusions in cast Al–Si alloys. Eng Fract Mech 2003;70:1281–302.
[14] Xue Y, El Kadiri H, Horstemeyer MF. Micromechanisms of multistage fatigue crack growth in a high-strength aluminum alloy. Acta Mater 2007;55:1975–84.